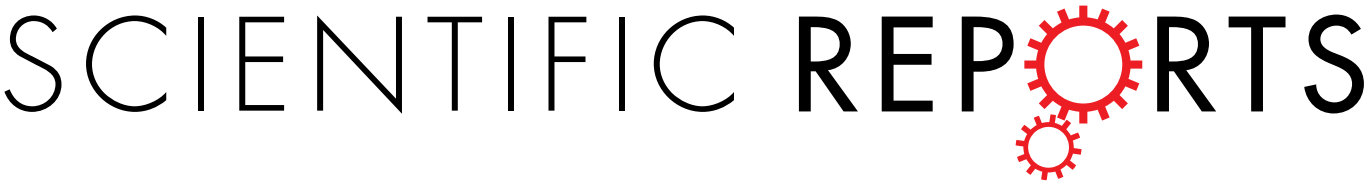

OPEN

Multi-Shell Hollow Nanogels with Responsive Shell Permeability

Andreas J. Schmid[1], Janine Dubbert[1], Andrey A. Rudov[2,3], Jan Skov Pedersen[4], Peter Lindner[5], Matthias Karg[6], Igor I. Potemkin[2,3] & Walter Richtering[1]

Received: 09 December 2015
Accepted: 18 February 2016
Published: 17 March 2016

We report on hollow shell-shell nanogels with two polymer shells that have different volume phase transition temperatures. By means of small angle neutron scattering (SANS) employing contrast variation and molecular dynamics (MD) simulations we show that hollow shell-shell nanocontainers are ideal systems for controlled drug delivery: The temperature responsive swelling of the inner shell controls the uptake and release, while the thermoresponsive swelling of the outer shell controls the size of the void and the colloidal stability. At temperatures between 32 °C $< T <$ 42 °C, the hollow nanocontainers provide a significant void, which is even larger than the initial core size of the template, and they possess a high colloidal stability due to the steric stabilization of the swollen outer shell. Computer simulations showed, that temperature induced switching of the permeability of the inner shell allows for the encapsulation in and release of molecules from the cavity.

A key challenge in the field of current biomedical research is the development of carrier systems, which allow for the uptake, storage and triggered release of functional agents. In this respect, hollow carriers made of stimuli-responsive polymers have gained significant interest in the last years. A crucial requirement for the design of such drug delivery systems is the (colloidal) stability of such nanocontainers and the cargo under physiological conditions as unspecifically released drugs can be metabolized and discharged from the body before reaching the desired location[1,2].

Dendrimers[3], micelles[4–6], nanohydrogels[2,7] and gold nanoparticles[8] were successfully used as drug delivery systems using a variety of stimuli for the release of the drugs as, e.g., light, pH, ultrasound or magnetic field. Moreover mesoporous silica nanoparticles were often used for drug delivery due to their biocompatibility, cost-efficient synthesis and surface modification as well as high loading capacity inside the mesoporous channels, although they face the problem of premature drug release[9,10].

A possible way to overcome this uncontrolled release is the use of responsive materials which allow for blocking of release pathways, i.e. via controlling the mesh size of a polymeric matrix. In this respect, hollow capsules represent a very promising structure for the design of efficient drug delivery systems[1,11,12]. Drugs could be stored in the void of the hollow particles with the shell protecting them from external influences but also a controlled release of the drugs by external stimuli is possible[13–17].

The use of a temperature sensitive polymer as a shell material offers switchability of the mesh size in the shell, and thus the permeability can easily be altered by temperature. Poly(*N*-isopropylacrylamide) (PNIPAm) shows a volume phase transition (VPT) in aqueous solution at about 32 °C[18]. This volume phase transition temperature (VPTT) can be adjusted by incorporation of comonomers[19] or functional comonomers like weak acidic[20–22] or basic[23,24] monomers, which also introduce a second stimulus, e.g. pH in this case.

The preparation of hollow particles follows usually a two-step procedure: In the first step, core-shell particles (CS) with a core are synthesized, and then the core can be chemically removed in the second step. Silica nanoparticles are often used as such sacrificial cores as they can be synthesized with in a broad range of sizes and very narrow size distributions[25]. Furthermore silica cores can easily be dissolved leading to hollow capsules[26–29].

In the past the structure of hollow PNIPAm nanogels was mainly studied by transmission electron microscopy (TEM) and the void size was regarded to be equal the initial core size. Recently, Dubbert *et al.*[30] investigated the

[1]Institute of Physical Chemistry, RWTH Aachen University, Landoltweg 2, 52056 Aachen, Germany. [2]Physics Department, Lomonosov Moscow State University, 119991 Moscow, Russian Federation. [3]DWI-Leibnitz Institute for Interactive Materials e.V., 52056 Aachen, Germany. [4]Interdisciplinary Nanoscience Center (iNANO) and Department of Chemistry, Aarhus University, 8000 Aarhus, Denmark. [5]Institut Laue Langevin (ILL), 71 avenue des Martyrs, 38000 Grenoble, France. [6]Physical Chemistry I, University of Bayreuth, 85440 Bayreuth, Germany. Correspondence and requests for materials should be addressed to I.I.P. (email: igor@polly.phys.msu.ru) or W.R. (email: richtering@rwth-aachen.de)

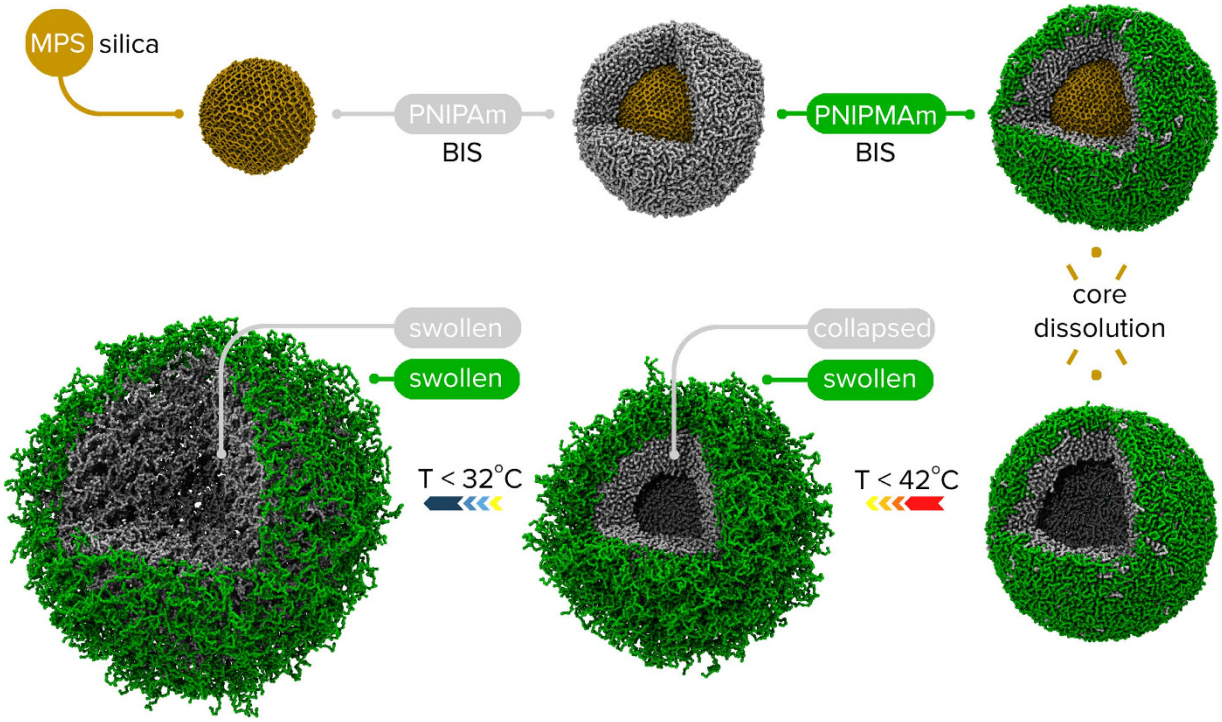

Figure 1. Scheme of the synthesis process of the doubly temperature-responsive core-shell-shell nanogels and hollow shell-shell nanogels.

internal structure of pitted PNIPAm particles by small-angle neutron scattering (SANS) and contrast variation experiments. They studied the effect of temperature, crosslink density in the shell and shell thickness on the void size. The authors could show, that above and below the VPTT of PNIPAm the polymer shell swells into the void. For slightly crosslinked polymer shells, the pitted particles showed a temperature-dependent swelling but did nearly not exhibit any void. In contrast pitted particles with a highly crosslinked polymer shell can be considered as hollow, but the particles were less temperature sensitive. However, for all scenarios the void in the pitted particles was smaller as compared to the size of the initial core.

A clever way to address this compromise between available void space and responsivity is the introduction of a second, outer polymer shell. Recently we described the synthesis of core-shell-shell (CSS) and the corresponding hollow shell-shell (HSS) nanogels[31]. We added a second crosslinked polymer shell consisting of poly(*N*-isopropylmetharcylamide) (PNIPMAm) on silica-PNIPAm core-shell particles. PNIPMAm shows a similar temperature sensitive behaviour in water as PNIPAm, but with a slightly higher VPTT of about 42 °C[32].

It is worth mentioning that both shells consist of uncharged polymers and thus tolerate the presence of salt. Therefore the swelling of the core-shell-shell and hollow shell-shell nanogels as well as the colloidal stability at intermediated temperatures is not sensitive to the ionic strength of the aqueous medium. This makes such temperature sensitive hollow shell-shell nanogels distinctly different from e.g. nanocapsules based on Layer-by-Layer adsorption of polyelectrolytes.

At temperatures above 42 °C both shells are collapsed, whereas at temperatures below 32 °C both shells are swollen by the solvent. At intermediate temperatures (32 °C $< T <$ 42 °C) only the outer PNIPMAm shell is swollen, while the inner PNIPAm shell is still collapsed (see Fig. 1). The collapsed inner shell also provides a significant cavity inside the hollow shell-shell particles as it hinders the outer shell from swelling into the void.

This could indeed be a promising system, e.g., for drug delivery, as it can provide a nanocontainer with a significant void together with temperature-controlled permeability of the inner PNIPAm shell and a high colloidal stability due to the outer, swollen PNIPMAm shell. The presence of the void can provide storage of both hydrophilic and hydrophobic guest molecules whose penetration into the void is not necessarily driven by long range Coulomb attraction like in the case of binding of charged molecules to oppositely charged carrier[33,34]. The uptake of the molecules can be achieved via diffusion through the shells of the HSS nanogel immersed in solution of the guest molecules with their subsequent arrest via locking the permeability of the inner shell.

In this work, we investigate the structure of hollow nanogels with two shells and their potential for controlled storage and release of cargo by a combination of SANS and molecular dynamics (MD) simulation for the first time.

The unique possibility of contrast variation in SANS allowed us to gain quantitative data on the structure of CS and CSS particles with silica cores in comparison to the respective hollow systems (HS and HSS) in solution. A core-shell form factor model[30] was extended and fitted to the experimental data to gain quantitative information about the shell thickness and void size at different temperatures: At 20 °C, where both polymer shells are swollen,

	20 °C		40 °C		52 °C	
	R_h [nm]	R [nm]	R_h [nm]	R [nm]	R_h [nm]	R [nm]
Core	70 ± 4	63 ± 4		—		—
CS	267 ± 13	270 ± 14	150 ± 8	130 ± 7	150 ± 8	—
CSS	355 ± 18	320 ± 18	269 ± 13	236 ± 12	187 ± 9	160 ± 8
HS	268 ± 13	248 ± 13	147 ± 7	127 ± 7	144 ± 7	—
HSS	387 ± 19	307 ± 16	269 ± 13	245 ± 13	179 ± 9	158 ± 8

Table 1. Hydrodynamic radii R_h[31] and particle radii R (compare equation (18)) from fitting the experimental scattering curves of the silica core, CS, CSS, HS and HSS particles in D_2O at 20 °C, 40 °C and 52 °C.

at 40 °C, where the inner PNIPAM shell is collapsed and the outer PNIPMAm shell is still swollen and at 52 °C, where both polymer shells are collapsed.

We performed MD simulations of CSS and HSS systems under analogues conditions, which revealed a good agreement between the experimental and computer simulation results. In addition MD simulations revealed the high efficiency of the HSS nanogels for uptake, storage and release of neutral species under different external conditions.

Results

In the following we report on the structure of the various particles as probed by SANS (Table 1 summarizes all fit results and all fitting parameters are given in Table S1) and MD simulation.

The scattering data of the silica core (see Fig. S1 in the Supporting Information) show that the silica core has a size of 63 nm and a narrow size distribution of 13%. These experimentally determined values of the silica core were used in the following to evaluate the scattering curves of the core-shell particles.

Structure of CS and HS nanogels. The structure of CS particles and the hollow nanogels will be compared above (40 °C) and below (20 °C) the VPTT of PNIPAm. To do so, the CS particles were measured at the scattering length density match point of the silica core (62 wt% D_2O in D_2O/H_2O mixture[30]) and the hollow nanogels at full scattering contrast in D_2O.

The scattering curves of the CS particles at the match point of the core and of the HS particles at 40 °C are depicted in Fig. S2a in the Supporting Information and show no significant difference in the collapsed state indicating the same microscopic structure of the PNIPAm shell. Both scattering profiles decay with q^{-4}, where q is the modulus of the scattering vector, in the high q-regime (except for the presence of a small constant background) pointing to a sharp particle-solvent interface. The PNIPAm shell can be described by a box profile for both, the CS and the HS particles, with a thickness of 67 nm (compare Fig. 2).

The void size of the hollow HS particles in the collapsed state is 60 nm and thus slightly smaller as the initial core size (63 nm) indicating a slight penetration of the PNIPAm shell into the void in collapsed state.

A more complex behaviour is observed below the VPTT of PNIPAm. Already a qualitative comparison of the q-dependent scattering intensity $I(q)$ of the core-matched CS and the HS particles in swollen state provides significant evidence for the presence of different shell structures. The first local minimum in the scattering profile of the core-shell particles is more smeared out as compared to the HS particles whereas the second minimum is more pronounced. The slope in the high-q-range is different for the CS and the HS particles, respectively and in both cases the slope is different from q^{-4}. The latter indicating a fuzzy particle surface.

The scattering curve of the CS particles at 20 °C can be described using a 2-step profile for the PNIPAm shell. The PNIPAm shell consists of a dense polymer layer with a thickness of ca. 10 nm next to the silica core and of a highly swollen layer with a thickness of 197 nm (see Fig. 2). The dense layer could be due to the adsorption of PNIPAm segments on the silica surface similar to the case when the silica nanoparticles serve as adhesives for gels and biological tissues[35]. The presence of this dense layer, however, will not be discussed in the following as this effect is not important for the structural behaviour of the systems presented in this study.

There are two major differences of structure of the hollow shell (HS) nanogel in the swollen state as compared to the CS system: (i) The inhomogeneity of the PNIPAm shell is less pronounced. In fact a fit with a 2-step profile revealed only slightly better results as compared to a fit with only one polymer shell, see Fig. S3. (ii) More importantly, the PNIPAm shell penetrated into the void (Fig. 2). In the swollen state, the void size (26 ± 3 nm) is *smaller* than the initial core volume (63 nm).

Structure of core-shell-shell (CSS) and hollow shell-shell (HSS) nanogels. Now, the effect of a second polymer shell, namely the PNIPMAm shell, on the internal structure will be investigated. The scattering curves $I(q)$ of the core-matched CSS particles will be compared to the scattering curves of the HSS particles at three temperatures: at 52 °C, which is above the VPTTs of both polymers, at 40 °C, which is above the phase transition temperature of PNIPAm but below the VPTT of PNIPMAm and at 20 °C, which is far below the VPTTs of PNIPAm and PNIPMAm.

At 52 °C, the scattering curves of the CSS particles (core-matched) and the HSS nanogels shown in Fig. S2 in the Supporting Information look very similar indicating rather similar shell structures with and without the silica core. The scattering data could be fitted with box profiles for both shells with sharp interfaces between the two polymer shells and between the PNIPAm shell and the silica core in case of the core-shell-shell particles.

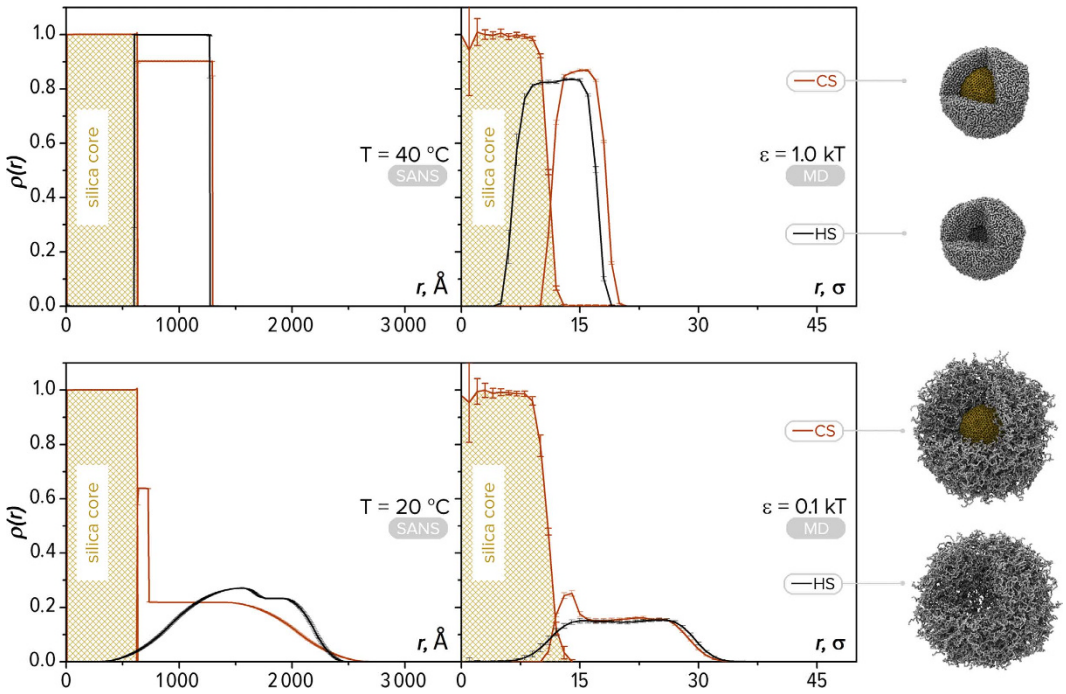

Figure 2. Radial density profiles $\rho(r)$ of the core-shell particles (CS) and of the hollow spheres (HS) particles. Experimentally obtained density profiles from SANS measurements (**left column**) of the CS particles at the match point (MP) of the silica core and of the HS nanogels at full scattering contrast in D_2O and from MD simulations (**right column**) at 40 °C (**top row**, bad solvent quality for the shell, $\varepsilon = 1$ in MD) and at 20 °C (**bottom row**, good solvent quality for the shell, $\varepsilon = 0.1$ in MD). The snapshots on the right represent equilibrium structure of nanogels obtained by MD.

The thickness of the PNIPMAm shell was determined to be 30 nm at 52 °C, which is rather thin compared to the inner PNIPAm shell (67 nm). The density profiles depicted in Fig. 3 reveal, that dissolving the silica core slightly affects the shell structures. The void in the HSS nanogel is 69 nm and thus slightly larger as the initial silica core size of 63 nm. This indicates that the outer PNIPMAm shell acts like an "inverse corset" and prevents the inner PNIPAm shell from penetrating into the void as it was observed without the second shell. This goes along with a compression of the outer shell, which can be seen as well in the density profile of the HSS nanogels, where the second shell is thinner and denser as for the CSS particles. The overall sizes of the HSS (158 nm) and the CSS particles (160 nm) are very similar.

At 40 °C, the outer PNIPMAM shell is expected to be swollen, whereas the inner PNIPAm shell is still collapsed. At this temperature, the SANS profiles exhibit clear differences between the HSS and CSS systems. The second local minimum in $I(q)$ of the HSS nanogels is shifted to higher q values as compared to the CSS particles measured at the matchpoint of silica. Also the slope of $I(q)$ in the high q-regime is different.

The density profiles of the CSS and HSS nanogels reveal a collapsed inner PNIPAm shell with sharp interfaces towards the core or the void, respectively, and to the outer PNIPMAm shell, which is highly swollen.

However, the radius of the void (76 nm) of the HSS nanogel at 40 °C is significantly larger than the radius of the silica core in the CSS system (63 nm) and also larger as compared to the void of the HS nanogel (radius 60 nm).

The PNIPMAm shell swells outwards and "pulls" the inner shell with it and the void size is *bigger* than the initial core size.

The scattering curves at 20 °C look even more complex as compared to the higher temperatures. The HSS nanogels show clearly two local minima in $I(q)$, whereas the first minimum is not present in the scattering curve of the CSS particles. Also the slope at high q is different for the HSS nanogels compared to the CSS system.

The density profile of the CSS particles (Fig. 3) reveals two swollen polymer shells and a dense polymer layer next to the silica core, similar to the CS particles at 20 °C (Fig. 2). After core dissolution, the inner PNIPAm shell intrudes the void. The size of the cavity is 25 ± 8 nm if only the completely polymer-free space is regarded as cavity and is similar to the hollow shell nanogel (26 ± 3 nm).

Thus, the swelling of the inner PNIPAm shell at 20 °C is less affected by the outer PNIPMAm shell as compared to 40 °C where the inner shell is collapsed.

Structures of CSS and HSS nanogels obtained from molecular dynamics simulations. We will now compare our experimental findings with the results from computer simulations. For that purpose we performed MD calculations of CSS/HSS particles with similar shells characteristics as in the experiment and with a crosslinker content of 4% in both shells (see section Computer simulations in details).

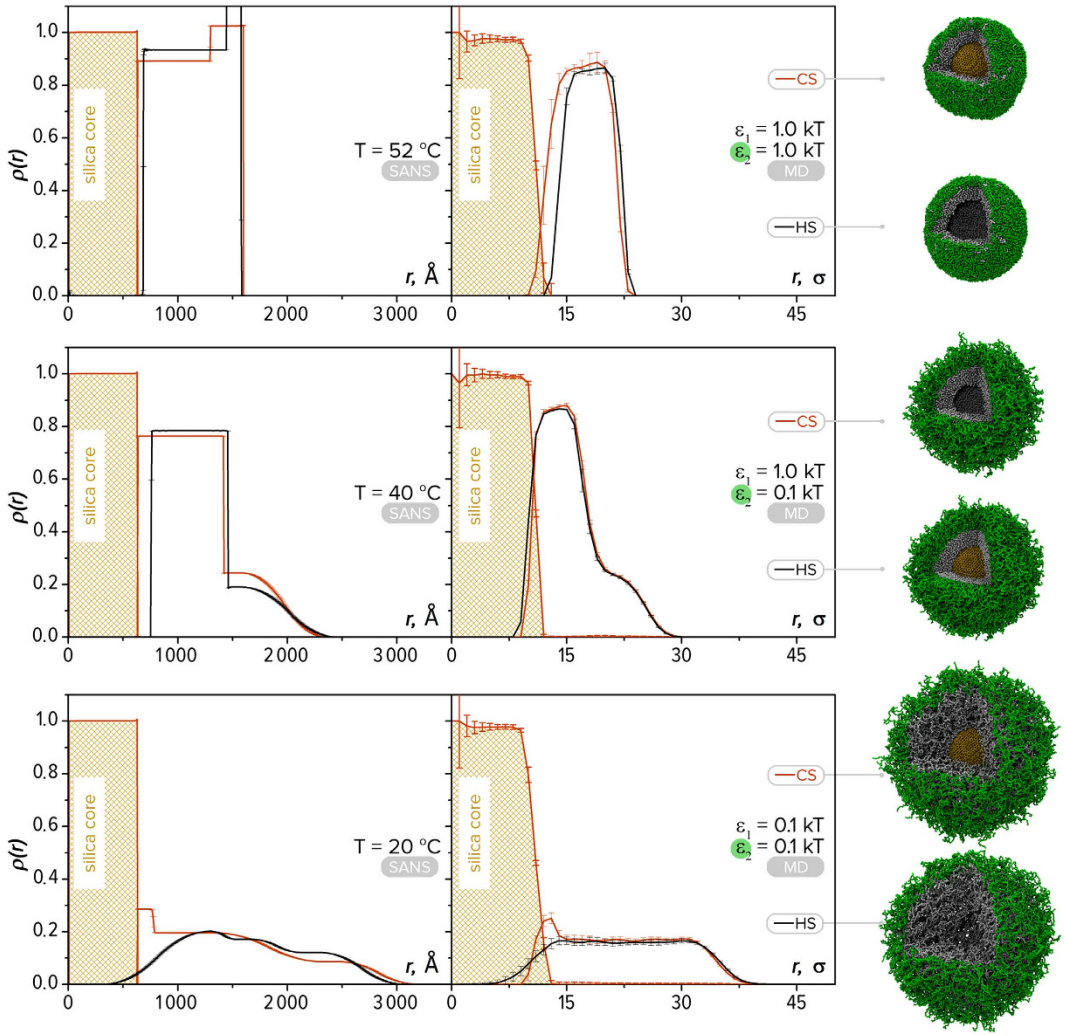

Figure 3. Radial density profiles $\rho(r)$ of the core-shell-shell particles (CSS) and of the hollow shell-shell nanogels (HSS). Experimentally obtained density profiles from SANS measurements (**left column**) of the CSS particles at the match point (MP) of the silica core and of the HSS nanogels at full scattering contrast in D_2O and from MD simulations (**right column**) at 52 °C (**top row**, the solvent is bad for both shells, $\varepsilon_1 = 1, \varepsilon_2 = 1$ in MD), at 40 °C (**middle row**, the solvent is bad for the inner shell and good for the outer shell, $\varepsilon_1 = 1, \varepsilon_2 = 0.1$ in MD) and at 20 °C (**bottom row**, the solvent is good for the both shells, $\varepsilon_1 = 0.1, \varepsilon_2 = 0.1$ in MD). The snapshots on the right represent equilibrium structure of nanogels obtained by MD.

In the simulations we use implicit solvent model. The swelling of the temperature sensitive shells is tuned by the Lennard-Jones interaction parameters, ε_1 and ε_2, which determine the solvent quality for the polymer shells. We used three different combinations for the solvent qualities in order to compare the results from simulations to the experimental ones: (a) a good solvent quality for both shells (referring to 20 °C in the experiment), (b) a solvent quality, which is good for the outer shell and bad for the inner shell (referring to 40 °C in the experiment) and (c) a situation with bad solvent conditions for both shells (referring to 52 °C in the experiment).

The calculated equilibrium structures of the CSS and HSS particles are shown in Figs 3 and 4 and the resulting density profiles are depicted in Fig. 3.

The density profiles of the two polymer shells at bad solvent conditions, $\varepsilon_1 = 1$ and $\varepsilon_2 = 1$, demonstrate high polymer volume fractions in the shells (maximum values in the inner and outer shells are more than 0.8 and 0.7, respectively) both for the CSS and HSS particles. The void size of the HSS nanogels is larger than the initial core size. Also, the second shell makes the void larger in comparison with the case of single-shell particle (HS), Fig. 4, which is a consequence of the increased bending modulus of the shell-shell system. These results are in good agreement with the experimental data.

Improving the solvent quality for the outer shell ($\varepsilon_1 = 1$, $\varepsilon_2 = 0.1$) leads to its swelling, i.e. decrease of the concentration of beads. This process is accompanied by a decrease of the size of the cavity up to the value of the solid core due to a reduction of the bending modulus of the outer shell. The concentration of beads inside the inner shell and its thickness remain practically the same (like in the case of bad solvent for both shells). It has to be mentioned that the average values of the polymer concentration in the shells quantitatively support the experimental

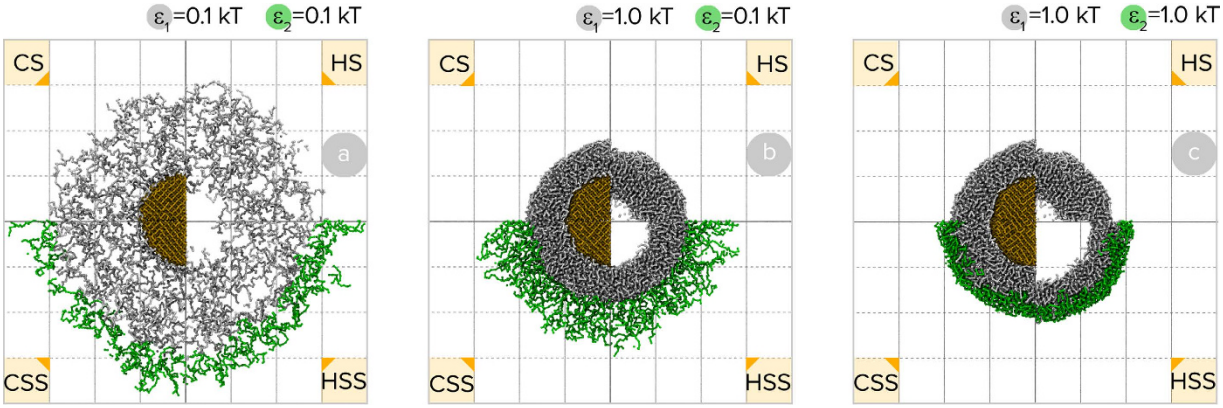

Figure 4. Equilibrium structures of the particles. Cross-sections through the centre of mass of the CS (upper left quarter), HS (upper right quarter), CSS (lower left quarter) and HSS (lower right quarter) nanogels where both shells contain 4% of crosslinker at solvent qualities where (**a**) both shells are swollen, $\varepsilon_1 = 0.1$, $\varepsilon_2 = 0.1$, (**b**) the inner shell is collapsed and the outer shell is swollen, $\varepsilon_1 = 1.0$, $\varepsilon_2 = 0.1$ and (**c**) both shells are collapsed, $\varepsilon_1 = 1.0$, $\varepsilon_2 = 1.0$.

data. The polymer concentration of the second shell is clearly enhanced at the interface between the two shells for the particles with and without core. The physical reason for that is shielding of unfavourable contacts of the inner shell with the solvent via adsorption of beads of the outer shell at the interface[36]. The inner shell slightly penetrates into the void, as the void is slightly smaller after removal of the core. However, two important differences between simulation and experiment have to be noticed: First, the experimentally determined density profiles do not exhibit a dense polymer layer of the second shell at the shell-shell interface. In the experimental system, the swelling of the second shell "pulls" the inner shell outwards and the void size is larger than the initial core size.

At good solvent conditions for both shells ($\varepsilon_1 = 0.1$, $\varepsilon_2 = 0.1$) also the inner shell swells which leads to a dense polymer layer next to the core in case of the CSS particles. The inner shell also swells clearly into the void after removal of the core (HSS particles). The enhancement of polymer density at the shell-shell interface at intermediate solvent conditions, however, disappeared regardless of the presence of a core. Very similar density profiles were obtained from the SANS experiments.

The removal of the core does not affect the overall size of the particles, as the size of the CSS and the HSS particles is approximately equal at all solvent conditions. This is also true for the experimental system, with the exception, that at 20 °C the HSS nanogels are slightly smaller compared to the CSS particles.

We can conclude, that the results from computer simulations agree very well with the experimental results. Thus computer simulations can be used to obtain reliable predictions of structural properties of such complex particles. It has to be noted that the MD simulation technique with implicit solvent does not restrict generality of consideration of similar systems in comparison with other models employing explicit solvent. In particular, recent computer simulations of hollow nanogels with the dissipative particle dynamics (DPD) also reveal stability of the cavity in the case of adsorption of such particles at liquid interface[37] In the following, we will demonstrate using the MD simulations that the designed HSS nanogels can efficiently be used for uptake, storage and release of neutral guest molecules.

The loading of short, soluble linear guest chains ($n = 5$, $\varepsilon_{gg} = 0.1$, see computer simulations for details) into the void of the HSS nanogels was modelled as follows. The solvent was considered to be good for both shells of the HSS nanogel ($\varepsilon_1 = 0.1$, $\varepsilon_2 = 0.1$) resulting in swelling and consequently high permeability of the shells. The guest chains were added into the outer (with respect to the nanogel) solvent, which penetrate into the nanogel. The snapshot in Fig. 5a demonstrates the distribution of the guest after 50×10^6 simulation steps. One can see that the average concentration of the chains in the cavity is approximately equal to the average concentration outside the nanogel. This result manifests a penetration of the linear chains into the nanogel void despite of excluded volume repulsion from the beads of the shell. To hold the chains in the nanogel while keeping the particle colloidaly stable, we make the solvent bad for the inner shell and good for the outer shell ($\varepsilon_1 = 1$, $\varepsilon_2 = 0.1$). The equilibrium structure of the nanogel is shown in Fig. 5b. We observe a significant increase of the concentration of the guest molecules in the cavity. This is due to a partial release of the chains from the collapsed inner shell into the cavity. In order to demonstrate the ability of the inner shell to keep the molecules inside the cavity, the nanogel was "cut" from the solution of the linear chains, Fig. 5b, "washed out" in pure solvent via removal of the guest chains from the outer shell and placed into pure solvent. Figure 5c depicts the structure of the system after 50×10^6 simulation steps. A negligible number of the guest chains leaves the nanogel (they are not visible in the snapshot, which is a cross section through the centre of mass and represents a small volume of the system) while the majority is trapped.

Therefore, the molecules can be delivered with the nanogel at this state and one can assume that they are reliably protected from interactions with surroundings by the dense shell. Easy release of the guest molecules is demonstrated in Fig. 5d when the solvent becomes again good for the inner shell ($\varepsilon_1 = 0.1$, $\varepsilon_2 = 0.1$). Thus, the proposed simulations demonstrate a straightforward way of using the designed HSS capsules as responsive

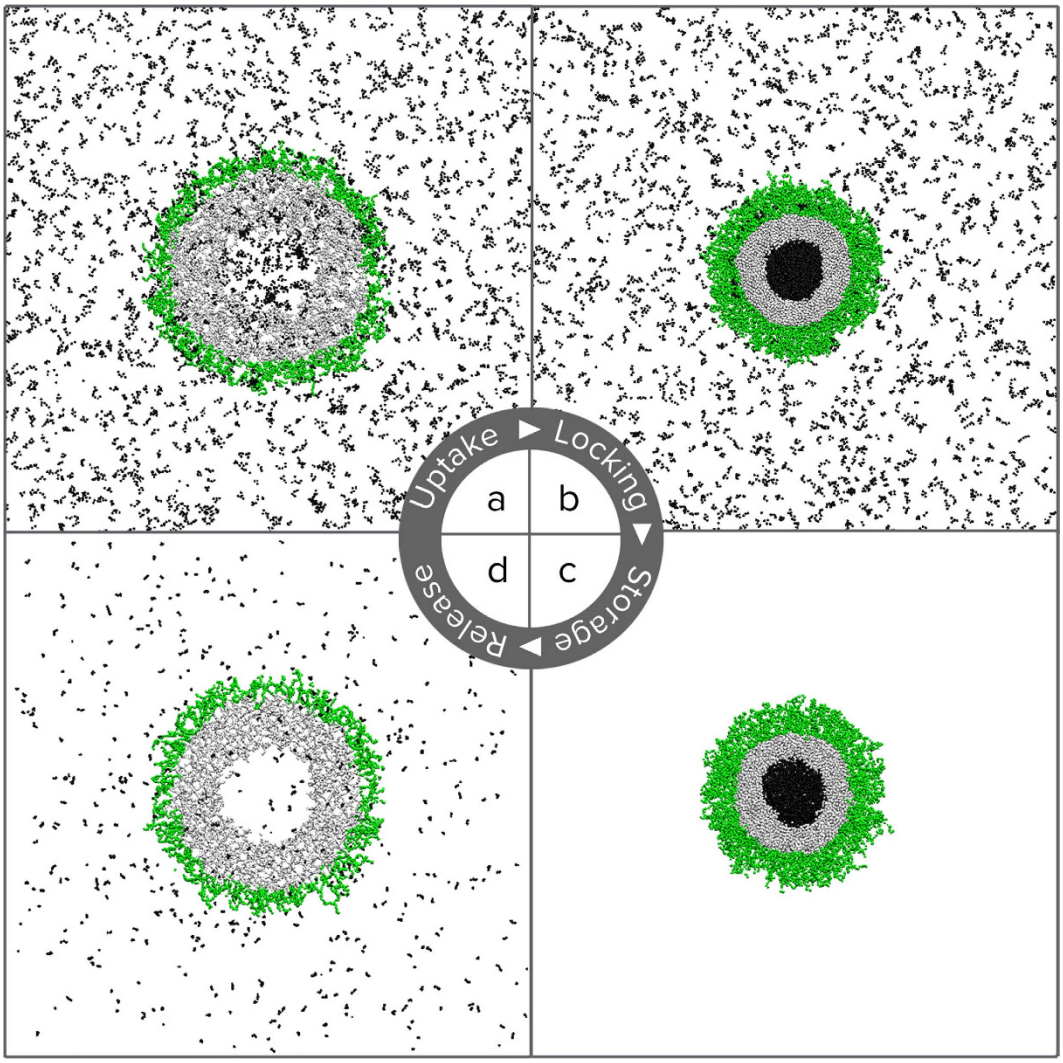

Figure 5. Equilibrium structures of the HSS nanogel with dissolved guest chains under different conditions: (**a**) Diffusion of the guest chains into the swollen nanogel ($\varepsilon_1 = 0.1, \varepsilon_2 = 0.1$); (**b**) Locking of the guest chains in the cavity via collapsing of the inner shell ($\varepsilon_1 = 1, \varepsilon_2 = 0.1$); (**c**) ability of the HSS nanogel with collapsed inner shell to hold the chains in the cavity ($\varepsilon_1 = 1, \varepsilon_2 = 0.1$); (**d**) Release of the guest chains from the HSS nanogel after swelling of the inner shell ($\varepsilon_1 = 0.1, \varepsilon_2 = 0.1$). The number of simulation steps was 50×10^6.

carriers. In the future we will use the predictions of computer simulations as guidance for experimental studies on the uptake and temperature-dependent release of neutral actives with different size.

Discussion

In this work we investigated the internal structure of core-shell-shell particles with two temperature-sensitive polymer shells (PNIPAm and PNIPMAM, respectively) with two different VPTTs and the corresponding hollow shell-shell particles experimentally by SANS and by MD simulations. Computer simulations were also used to predict their possible application as thermoresponsive nanocontainers for drug delivery.

Our results of the precursor particles, CS and HS, are similar to the results of Dubbert *et al.*[30] for particles with a rather thick and low crosslinked shell. The PNIPAm shell is able to penetrate into the void below and above the VPTT, but is more pronounced in swollen state. A reduced void size, of course, counteracts their use for drug delivery as the possible loading capacity is also reduced. This problem could be solved either by the preparation of larger particles[38,39], where the penetration of the shell into the void would be negligible, or nanocontaines with a highly crosslinked shell[30].

However, for the use as drug delivery systems the size of the nanocontainers is limited to a few hundreds of nanometres to allow their diffusion into the cells and for their intravenous or mucosal application[1,40]. A highly crosslinked shell might also hinder the release of the encapuslated drug.

In general, thermoresponsive nanocapsules for drug delivery should store the drug inside the cavity at body temperature, which is about 37 °C, and allow a quick release at, for example, locally heated tumour cells[1]. Up to now, liposomes offer the highest potential as thermoresponsive drug delivery systems. Despite of their numerous

advantages, e.g. high biocompatibility, possibility for uptake of hydrophilic and hydrophobic molecules and easy change of size or surface properties, they also show serious drawbacks, as the rapid elimination from the blood and clearance by the cells of the reticulo-endothelial system[41].

PNIPAm capsules are collapsed at 37 °C, which would favour the encapsulation of drugs, but only a release at temperatures below 32 °C, where the shell permeability is increased upon swelling of the PNIPAm shell. Lee *et al.*[42] showed an example of this so-called "cold shock" therapy. Nanocontaines based on Pluronic F127–polyethyleneimine were used to transfer small interfering RNA (siRNA) into the cytosol leading to the inhibition of the target messenger RNA. However, PNIPAm nanogels still face the problem of low colloidal stability in collapsed state under physiological conditions[43] and a higher toxicity in collapsed state as compared to the swollen nanogel[44]. Blackburn *et al.*[45] successfully used a PNIPMAm nanogel for siRNA delivery into ovarian carcinomas. They observed a gene silencing in the cell interior and no significant toxicity of the nanogel construct.

Considering the points given in the previous section, one can infer that a hollow capsule with two polymer shells, where the temperature responsive swelling of the inner shell controls the uptake and release and a swollen outer shell provides the colloidal stability, would therefore be an ideal system for controlled drug delivery.

In the present work, we could show with experiments and computer simulations that HSS nanogels meet the requirements for their use as drug delivery systems. At temperatures between $32\,°C < T < 42\,°C$, which covers the body temperature of 37 °C, the particles provide a significant void, which is even larger as the initial core size, and a high colloidal stability at high ionic strengths, which are typically found in the human body, due to the steric stabilization of the swollen outer shell. Computer simulations also showed, that switching the permeability of the inner shell can be used for the encapsulation of active species as well as for a triggered release.

Methods

Chemicals. Deuterated water (D_2O, 99.9%) was obtained from Deutero.

Synthesis. The synthesis of the core-shell-shell (CSS) and the hollow shell-shell (HSS) nanogels was previously described[31]. In brief, silica particles were prepared in a Stoeber synthesis[25] in a three-neck round-bottom flask equipped with a reflux condenser. 11 mL of ammonia solution were mixed with 130 mL ethanol and equilibrated at 50 °C. The reaction was started by addition of a preheated solution of 5 mL tetraethylorthosilicate (TEOS) in 15 mL ethanol. After 12 h of reaction time, the surface of the silica nanoparticles was modified with 3-(trimethoxysilyl)propylmethacrylate (MPS)[46]. The particles were purified by centrifugation and redispersion in fresh solvent. Simultaneously, the concentration of the silica nanoparticle stock solution was increased by a factor of 10.

The first shell was added on the silica core in the following manner: 1.075 g NIPAm (9.5 mmol, 94.9 mol%), 0.0788 g BIS (0.5 mmol; 5.1 mol%) as crosslinker and 0.1 g polyvinylpyrolidone (PVP) as stabilizer were mixed in 100 mL water and degassed. One fourth of the silica stock solution was added and the reaction was initiated with 1 mL of a potassium persulfate (PPS) solution (10 mg/mL). After purification by centrifugation and redispersion, the core-shell (CS) particles were freeze-dried.

The core-shell-shell (CSS) particles were synthesized by conducting a second polymerization step: A stock solution containing 20.5 g NIPMAm (161.2 mmol; 96.5 mol%), 0.89 g BIS (5.8 mmol; 3.5 mol%) and 1.22 g sodium dodecylsulfate (SDS) as stabilizer was prepared in 670 mL of bidistilled water. 16.8 mL of the stock solution were diluted with 25.2 mL of water and the solution was heated to 70 °C and degassed with nitrogen. 200 mg of the freeze-dried CS particles were dissolved in 15 mL of water and added to the mixture. After equilibration of the solution, the reaction was started by the addition of 10 mL PPS solution (1 mg/mL) and carried out for 4 h under continuous stirring and nitrogen flow. The CSS particles were cleaned by three cycles of centrifugation/redispersion and finally lyophilized.

Hollow nanogels (HS) were prepared as reported previously[30]. Lyophilized CS particles were stirred overnight in highly diluted hydrofluoric acid (HF) followed by extensive dialysis against water and lyophilisation.

One fourth of the CSS particles were dissolved in 20 mL of a 50 mM NaOH solution to prepared hollow nanogels with two shells (HSS). The reaction was performed at 42 °C for 72 h to achieve complete core dissolution at a sufficient dissolution rate[47]. The HSS nanogels were purified by dialysis against 50 mM NaOH and water until a neutral pH was reached. The final material was freeze-dried.

Small Angle Neutron Scattering (SANS). Experiments were performed at the instrument D11 at the Institut Laue-Langevin (ILL) in Grenoble, France[48]. Wavelengths of $\lambda = 6$ Å and $\lambda = 17$ Å with a polydispersity of $\Delta\lambda/\lambda = 9\%$ were used. Samples were measured at three sample-detector distances of 1.2 m, 8 m and 39 m to cover the entire available range of the modulus of the scattering vector, q, of the instrument. The scattering intensity was detected on a ^{3}He gas detector (CERCA) with a detection area of $96 \times 96\,cm^2$ and a pixel size of $3.75 \times 3.75\,mm^2$. Narrow Hellma quartz glass cells (type 110-QS) with 2 mm sample thickness were used. The incoherent scattering of water was measured as secondary calibration standard at 8 m sample-detector distance. All data were corrected for transmission, empty cell scattering and background scattering to receive absolute values for the differential cross section.

The samples were measured in a copper sample changer at 20 °C, 40 °C and 52 °C. The sample temperature was measured inside a cell filled with water by an external thermometer and adjusted by an external thermostat. A dilute solution of the silica core was measured and the concentration was about 0.5 mg/mL for all other samples. Previous light, X-ray and neutron scattering experiments performed on core-shell microgels as well as on hollow microgels revealed that the structure of the microgels is fully reversible with temperature[30,31,49,50]. Furthermore heating-cooling cycles revealed no hysteresis. Thus the scattering data describe the equilibrium structure of the microgels in solution.

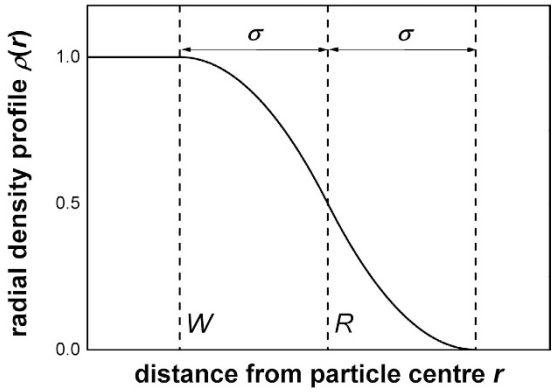

Figure 6. Schematic representation of a radial density profile $\rho(r)$ with gradual decaying surface (adapted from Stieger *et al.*[57]).

Measurements were performed at full scattering contrast (100% D_2O) and at a scattering contrast, where the silica core was matched (62 wt% D_2O in D_2O/H_2O mixture)[30].

Theoretical Background and Data Analysis. SANS experiments give the intensity distribution *I(q)* as a function of the modulus of the momentum transfer *q* in reciprocal space. A common way to express the intensity distribution *I(q)* is the use of the differential cross section $d\sigma(q)/d\Omega$. The differential cross section does not depend on the transmission and form of the sample and can generally be expressed as

$$I(q) = \frac{d\sigma}{d\Omega}(q) = nP(q)S(q) \tag{1}$$

n denotes the particle number density, *P(q)* is the particle form factor and *S(q)* is the structure factor, which represents interparticle correlations. In dilute solutions, particle-particle interactions can be neglected and thus $S(q) = 1$.

In SANS experiments, also the smearing of the instrument has to be taken into account. This smearing depends on the wavelength distribution and the finite collimation of the incoming neutron beam as well as the detector resolution.

A (Gaussian) probability function for the scattering vector *q* for a given nominal scattering vector $\langle q \rangle$ is added to the model expression for the differential cross section[49]

$$I^{\mathrm{mod}}(\langle q \rangle) = n \int_0^\infty R(\langle q \rangle, q) \frac{d\sigma}{d\Omega}(q) dq \tag{2}$$

In this study, we investigated the internal structure of doubly temperature-sensitive core-shell-shell and hollow shell-shell nanogel particles. Dubbert *et al.*[30] investigated the structure of core-shell and hollow nanogel particles. They could show that a second, highly crosslinked shell located at the core interface was necessary to fit the experimental scattering data. Consequently, we extended the model of Dubbert *et al.*[30], which is based on the core-shell model of Berndt *et al.*[50,51], by adding a third polymer shell.

In our case, the first polymer shell consists of crosslinked PNIPAm, too, and the second shell of crosslinked PNIPMAm. It was already shown for both pure nanogels, that due to the higher reaction rate of the crosslinker BIS, an inhomogeneous crosslink density is formed during the polymerization which leads to a gradual decaying surface of the particle in swollen state.

The radial density profile $\rho(r)$ of a particle with such an inhomogeneous crosslink density is schematically shown in Fig. 6 and can be expressed by the half-height radius $R = W + \sigma$.

$$\rho(r) = 1 \; r \leq (R - \sigma) \tag{3}$$

$$\rho(r) = 1 - \frac{1}{2}\frac{[(r - R) + \sigma]}{\sigma^2} \; (R - \sigma) < r \leq R \tag{4}$$

$$\rho(r) = 0 \; (R + \sigma) < r \tag{5}$$

$$\rho(r) = 0 \; (R + \sigma) < r \tag{6}$$

The Fourier transformation of this radial density profile leads to the scattering amplitude $\Phi(q, R, \sigma)$:

$$\Phi(q, R, \sigma) = \frac{1}{V_n}\left[\left(\frac{R}{\sigma^2}+\frac{1}{\sigma}\right)\frac{\cos(q(R+\sigma))}{q^4}+\left(\frac{R}{\sigma^2}-\frac{1}{\sigma}\right)\frac{\cos(q(R-\sigma))}{q^4} - \frac{3\ \sin(q(R+\sigma))}{q^5\sigma^2} - \frac{3\ \sin(q(R-\sigma))}{q^5\sigma^2} + \frac{2\ \cos(qR)}{q^5\sigma^2} + \frac{6\ \sin(qR)}{q^5\sigma^2}\right] \tag{7}$$

with $\Phi(q=0, R, \sigma)=1$.

The scattering amplitude of the core $A_{core}(q, R_{core}, \sigma_1, \Delta\rho_{core})$ with radius R_{core} and interface width σ_1 is the given by:

$$A_{core}(q, R_{core}, \sigma_1, \Delta\rho_{core}) = \Delta\rho_{core} V_{core} \Phi_{core}(q, R_{core}, \sigma_1) \tag{8}$$

where $\Delta\rho_{core}$ is the scattering length density and V_{core} the volume of the core.

The scattering amplitude of the shells can be expressed by differences of scattering amplitudes with different radii R and interface width σ.

$$A_{sh,1}\left(q, R_{sh,1}, \sigma_2, \Delta\rho_{sh,1}, R_{core}, \sigma_1\right) = \Delta\rho_{sh,1}(V_{sh,1}\Phi(q, R_{sh,1}, \sigma_2) - V_{core}\Phi(q, R_{core}, \sigma_1)) \tag{9}$$

$$A_{sh,2}(q, R_{sh,2}, \sigma_3, \Delta\rho_{sh,2}, R_{sh,1}, \sigma_2) = \Delta\rho_{sh,2}(V_{sh,2}\Phi(q, R_{sh,2}, \sigma_3) - V_{sh,1}\Phi(q, R_{sh,1}, \sigma_2) \tag{10}$$

$$A_{sh,3}(q, R_{sh,3}, \sigma_4, \Delta\rho_{sh,3}, R_{sh,2}, \sigma_3) = \Delta\rho_{sh,3}(V_{sh,3}\Phi(q, R_{sh,3}, \sigma_4) - V_{sh,2}\Phi(q, R_{sh,2}, \sigma_3) \tag{11}$$

$\Delta\rho_{sh,1}$ and $V_{sh,1}$ are the scattering length density and the volume of the first shell, $\Delta\rho_{sh,2}$ and V_{sh2} are the scattering length density and the volume of the second shell and $\Delta\rho_{sh,3}$ and $V_{sh,3}$ are the scattering length density and the volume of the third shell, respectively.

The scattering amplitude of the CSS particle with core and two shells is then be written as:

$$A(q) = A_{core}(q, R_{core}, \sigma_1, \Delta\rho_{core}) + A_{sh,1}(q, R_{sh,1}, \sigma_2, \Delta\rho_{sh,1}, R_{core}, \sigma_1) + A_{sh,2}(q, R_{sh,2}, \sigma_3, \Delta\rho_{sh,2}, R_{sh,1}, \sigma_2) + A_{sh,3}(q, R_{sh,3}, \sigma_4, \Delta\rho_{sh,3}, R_{sh,1}, \sigma_3) \tag{12}$$

The form factor $P(q)$ is the square of the scattering length amplitude $A^2(q)$.

The polydispersity of the core radius and the thickness of the polymer shell were taken into account separately by introducing a constant scale factor $\langle S\rangle$ of the overall particle size. A normalized Gaussian distribution describes this scale factor

$$D\left(S, \left\langle S\right\rangle = 1, \sigma_{poly}\right) = \frac{1}{\sqrt{2\pi\sigma_{poly}^2\left\langle S\right\rangle^2}}\exp\left(-\frac{(S-\langle S\rangle)^2}{2\sigma_{poly}^2\langle S\rangle^2}\right) \tag{13}$$

where $\langle S\rangle = 1$ is the average scale factor of the size and σ_{poly} is the relative particle size polydispersity. The form factor is convoluted with the size distribution by multiplying all size parameters in the model by S and performing the integral over S.

A Lorenzian function was added to the particle form factor to describe the scattering profile in the high q-regime of samples with swollen polymer shells:

$$I_L(q) = I_L(0)/[1 + q^2\xi^2] \tag{14}$$

This takes the internal structure of the polymer network into account where ξ represents the correlation length in the polymer shell network. A constant background I_{back} is needed to correct for residual incoherent scattering from the sample.

Incorporating all the contributions yields a model expression for the scattering intensity distribution

$$I^{mod}(\langle q\rangle) = n\int_0^\infty\int_0^\infty R(\langle q\rangle, q)\ D(S, \langle S\rangle, \sigma_{poly})\ [A^2(q) + I_L(q) + I_{back}]\ dS\,dq \tag{15}$$

with the number density

$$n = c\left[\int_0^\infty\left[\varphi_{core}\rho_{core}V_{core} + \varphi_{sh,1}\rho_{sh,1}V_{sh,1} + \varphi_{sh,2}\rho_{sh,2}V_{sh,2} + \varphi_{sh,3}\rho_{sh,3}V_{sh,3}\right]D(S, \langle S\rangle, \sigma_{poly})dS\right]^{-1} \tag{16}$$

c represents the polymer mass concentration, φ_i and ρ_i are, respectively, the volume fraction and the partial specific mass density of the i'th component, and the volumes have implicitly a dependence on the structural parameters as explained above.

The radial density profiles were calculated for the average particle by a numerical Fourier transformation of the scattering amplitude using the obtained volume fractions and scattering length densities:

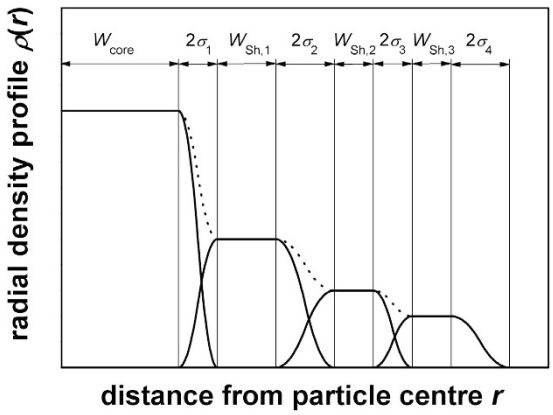

Figure 7. Schematic representation of the model used to fit the scattering data. The overall particle radius R is the point, where the density profile $\rho(r)$ approaches zero.

$$\rho(r) = \frac{1}{2\pi^2}\int A(q)\frac{\sin(qr)}{qr}q^2 dq \tag{17}$$

A schematic radial density profile $\rho(r)$ for a core-shell-shell-shell particle is depicted in Fig. 7. The point, where the density profile approaches zero is the overall particle radius R, which is calculated from the fitting parameters:

$$R = W_{\text{core}} + 2\sigma_1 + W_{\text{sh},1} + 2\sigma_2 + W_{\text{sh},2} + 2\sigma_3 + W_{\text{sh},3} + 2\sigma_4 \tag{18}$$

Computer simulations. The simulations were performed using LAMMPS[52]. Internal structures of the CSS and HSS nanogels were simulated using Brownian molecular dynamics simulation technique within a standard coarse-grained model with implicit solvent. All structural units of the nanogels (including core) were modeled as Lennard-Jones particles (beads) of the diameter σ and of the mass, m. The nanogels were designed as follows. First, we construct a unit cell of the diamond crystal lattice where the vertexes correspond to tetrafunctional crosslinkers connecting fully stretched subchains[53,54]. Then we assemble a cubic frame consisting of $9 \times 9 \times 9$ unit cells which is considered as a bar for the nanogel shells. The number of beads in each subchain (number of beads between two crosslinkers) was chosen to be 12. Considering that 4 halves of the subchains accounts for each tetrafunctional crosslinker the estimated fraction of the crosslinkers is $1/(4*6+1) = 0{,}04$. Three concentric spheres of different radii were inscribed into the cubic frame. They corresponded to boundaries of the outer, inner shells and solid core, respectively. All beads, which were outside the largest and inside the smallest spheres, were cropped and the rest beads were differentiated by their affiliation to the inner (white beads) and outer (green beads) shells (HSS). With this approach, the fractions of the crosslinkers in the outer and inner shells were equal. The thicknesses of the shells were controlled by the radii of the concentric spheres. The solid core of the core-shell-shel nanogel was also obtained on the basis of the diamond crystal lattice ($15 \times 15 \times 15$ unit cells). However, the subchains of the core consisted of only one bead and all the beads form a closely-packed system with attractive interactions between the beads. The spherical shape of the core is also provided via inscribing a sphere of appropriate radius into the frame and cropping all the beads which are outside the sphere. Attractive interactions between the beads of the core provide also attraction between different particles and high surface energy of the particles which one has in many nanoparticle systems without steric or electrostatic stabilization. Then the spherical core was inserted into the hole of the HSS particle with further grafting of the dangling ends to the core (CSS particle). The overall volumes of the beads in the outer shell, inner shell and the core were fixed and related to each other as 0.4:0.45:0.15, respectively. The interactions between any pair of beads were described through the truncated-shifted Lennard-Jones potential (see refs 55,56 for details). The value of the dimensionless Lennard-Jones interaction parameters ε_1, ε_2 and $\varepsilon_{12} = (\varepsilon_1\varepsilon_2)^{1/2}$, describing bead-bead interactions in the inner (ε_1), outer (ε_2) shells and between the shells (ε_{12}), were varied between 0.1 and 1 corresponding to repulsion (good solvent) and attraction (poor solvent), respectively. Attraction of the beads in the solid core was described by the interaction parameter $\varepsilon_0 = 0.33$ which also means that the solvent is poor for the particles. After fixing the primary structures of the nanogels, they were placed in a cubic simulation box of the volume $V = 500^3\ \sigma^3$ with periodic boundary conditions and subjected to annealing at different values of ε_1 and ε_2 (solvent quality for the shells). The calculations were carried out in NVT ensemble, which is quite efficient for models with implicit solvent. They last $50{\cdot}10^6$ simulation steps, which are enough to approach the equilibrium states of the system. In the computer simulations of uptake and release of neutral species, the guest molecules were considered as short linear chains of the number of beads $n = 5$ for which the solvent was always good. $M = 22000$ chains were admixed into a cubic simulation box of the volume $V = 150^3\ \sigma^3$ where the HSS nanogel was initially placed. The Lennard-Jones interaction parameters, describing pairwise interactions of the beads in the guest molecules with each other, ε_{gg}, and with the beads of the subchains of both shells (host), ε_{gh}, were fixed and corresponded to the exclude volume repulsion, $\varepsilon_{gg} = \varepsilon_{gh} = 0.1$. Loading, storage and release of the guest molecules were realized at different solvent

quality for the inner shell of the HSS nanogel. The system approached equilibrium state during each stage of the process, i.e., both loading, storage, and release were simulated during $50{\cdot}10^6$ simulation steps.

References

1. Mura, S., Nicolas, J. & Couvreur, P. Stimuli-responsive nanocarriers for drug delivery. *Nat Mater* **12,** 991–1003 (2013).
2. Nuhn, L. *et al.* Aggregation behavior of cationic nanohydrogel particles in human blood serum. *Biomacromolecules* **15,** 1526–1533 (2014).
3. Kurtoglu, Y. E. *et al.* Poly(amidoamine) dendrimer–drug conjugates with disulfide linkages for intracellular drug delivery. *Biomaterials* **30,** 2112–2121 (2009).
4. Yang, Y. Q., Zheng, L. S., Guo, X. D., Qian, Y. & Zhang, L. J. pH-sensitive micelles self-assembled from amphiphilic copolymer brush for delivery of poorly water-soluble drugs. *Biomacromolecules* **12,** 116–122 (2011).
5. Gao, G. H. *et al.* The use of pH-sensitive positively charged polymeric micelles for protein delivery. *Biomaterials* **33,** 9157–9164 (2012).
6. Cheng, Y. *et al.* Thermally controlled release of anticancer drug from self-assembled γ-substituted amphiphilic poly(ε-caprolactone) micellar nanoparticles. *Biomacromolecules* **13,** 2163–2173 (2012).
7. Nuhn, L. *et al.* Cationic nanohydrogel particles as potential siRNA carriers for cellular delivery. *ACS Nano* **6,** 2198–2214 (2012).
8. Dohnert, M. B. *et al.* Gold nanoparticles and diclofenac diethylammonium administered by iontophoresis reduce inflammatory cytokines expression in Achilles tendinitis. *Int J Nanomedicine* **7,** 1651–1657 (2012).
9. Liu, C. *et al.* Targeted intracellular controlled drug delivery and tumor therapy through *in situ* forming Ag nanogates on mesoporous silica nanocontainers. *ACS Appl. Mater. Interfaces* **7,** 11930–11938 (2015).
10. Yang, K. *et al.* Intracellular pH-triggered, targeted drug delivery to cancer cells by multifunctional envelope-type mesoporous silica nanocontainers. *ACS Appl. Mater. Interfaces* **7,** 17399–17407 (2015).
11. Amstad, E., Kim, S.-H. & Weitz, D. A. Photo- and thermoresponsive polymersomes for triggered release. *Angew. Chem. Int. Ed.* **51,** 12499–12503 (2012).
12. Windbergs, M., Zhao, Y., Heyman, J. & Weitz, D. A. Biodegradable core–shell carriers for simultaneous encapsulation of synergistic actives. *J. Am. Chem. Soc.* **135,** 7933–7937 (2013).
13. Stuart, M. *et al.* Emerging applications of stimuli-responsivepolymer materials. *Nature Materials* **9,** 101–113 (2010).
14. Skorb, E. V. & Möhwald, H. 25th Anniversary Article: dynamic interfaces for responsive encapsulation systems. *Adv. Mater.* **25,** 5029–5043 (2013).
15. Karamitros, C. S., Yashchenok, A. M., Möhwald, H., Skirtach, A. G. & Konrad, M. Preserving catalytic activity and enhancing biochemical stability of the therapeutic enzyme asparaginase by biocompatible multilayered polyelectrolyte microcapsules. *Biomacromolecules* **14,** 4398–4406 (2013).
16. Caruso, F., Trau, D., Möhwald, H. & Renneberg, R. Enzyme encapsulation in layer-by-layer engineered polymer multilayer capsules. *Langmuir* **16,** 1485–1488 (2000).
17. Masoud, H. & Alexeev, A. Controlled release of nanoparticles and macromolecules from responsive microgel capsules. *ACS Nano* **6,** 212–219 (2012).
18. Pelton, R. H. & Chibante, P. Preparation of aqueous latices with N-isopropylacrylamide. *Colloids and Surfaces* **20,** 247–256 (1986).
19. Keerl, M., Smirnovas, V., Winter, R. & Richtering, W. Interplay between hydrogen bonding and macromolecular architecture leading to unusual phase behavior in thermosensitive micirogels. *Angew. Chem. Int. Ed.* **47,** 338–341 (2008).
20. Snowden, M. J., Chowdhry, B. Z., Vincent, B. & Morris, G. E. Colloidal copolymer microgels of N-isopropylacrylamide and acrylic acid: pH, ionic strength and temperature effects. *J. Chem. Soc., Faraday Trans.* **92,** 5013–5016 (1996).
21. Jones, C. D. & Lyon, L. A. Shell-restricted swelling and core compression in poly (N-isopropylacrylamide) core-shell microgels. *Macromolecules* **36,** 1988–1993 (2003).
22. Kleinen, J. & Richtering, W. Defined complexes of negatively charged multisensitive poly (N-isopropylacrylamide-co-methacrylic acid) microgels and poly (diallydimethylammonium chloride). *Macromolecules* **41,** 1785–1790 (2008).
23. Cornelius, V. J., Snowden, M. J., Silver, J. & Fern, G. R. A study of the binding of the biologically important hematin molecule to a novel imidazole containing poly(N-isopropylacrylamide) microgel. *Reactive and Functional Polymers* **58,** 165–173 (2004).
24. Hu, X., Tong, Z. & Lyon, L. A. Synthesis and physicochemical properties of cationic microgels based on poly(N-isopropylmethacrylamide). *Colloid and Polymer Science* **289,** 333–339 (2010).
25. Stöber, W., Fink, A. & Bohn, E. Controlled growth of monodisperse silica spheres in the micron size range. *Journal of Colloid And Interface Science* **26,** 62–69 (1968).
26. Xing, Z. *et al.* Dual stimuli responsive hollow nanogels with IPN structure for temperature controlling drug loading and pH triggering drug release. *Soft Matter* **7,** 7992 (2011).
27. Lapeyre, V. *et al.* Multiresponsive hybrid microgels and hollow capsules with a layered structure. *Langmuir* **25,** 4659–4667 (2009).
28. Zha, L. S., Zhang, Y., Yang, W. L. & Fu, S. K. Monodisperse temperature sensitive microcontainers. *Adv. Mater.* **14,** 1090–1092 (2002).
29. Zhang, F., Hou, G., Dai, S., Lu, R. & Wang, C. Preparation of thermosensitive PNIPAM microcontainers and a versatile method to fabricate PNIPAM shell on particles with silica surface. *Colloid and Polymer Science* **290,** 1341–1346 (2012).
30. Dubbert, J. *et al.* How Hollow Are Thermoresponsive Hollow Nanogels? *Macromolecules* **47,** 8700–8708 (2014).
31. Dubbert, J., Nothdurft, K., Karg, M. & Richtering, W. Core-shell-shell and hollow double-shell microgels with advanced temperature responsiveness. *Macromol. Rapid Commun.* **36,** 159–164 (2015).
32. Kokufuta, M., Sato, S. & Kokufuta, E. LCST behavior of copolymers of N-isopropylacrylamide and N-isopropylmethacrylamide in water. *Colloid and Polymer Science* **290,** 1671–1681 (2012).
33. Kabanov, V. & Kabanov, A. Interpolyelectrolyte and block ionomer complexes for gene delivery: physico-chemical aspects. *Adv. Drug Deliv. Rev.* **30,** 49–60 (1998).
34. Vinogradov, S. V. Colloidal microgels in drug delivery applications. *Curr. Pharm. Des.* **12,** 4703–4712 (2006).
35. Rose, S. *et al.* Nanoparticle solutions as adhesives for gels and biological tissues. *Nature* **505,** 382–385 (2014).
36. Rudov, A. A. *et al.* Structural changes in lamellar diblock copolymer thin films upon swelling in nonselective solvents. *Macromolecules* **46,** 5786−5795 (2013).
37. Geisel, K., Rudov, A. A., Potemkin, I. I. & Richtering, W. Hollow and core-shell microgels at oil-water interfaces: spreading of soft particles reduces the compressibility of the monolayer. *Langmuir* **31,** 13145–13154 (2015).
38. Seiffert, S. Small but smart: sensitive microgel capsules. *Angew. Chem. Int. Ed.* **52,** 11462–11468 (2013).
39. Shah, R. K., Kim, J.-W., Agresti, J. J., Weitz, D. A. & Chu, L.-Y. Fabrication of monodisperse thermosensitive microgels and gel capsules in microfluidic devices. *Soft Matter* **4,** 2303 (2008).
40. Skorb, E. V. & Möhwald, H. 25th Anniversary Article: dynamic interfaces for responsive encapsulation systems. *Adv. Mater.* **25,** 5029–5043 (2013).
41. Torchilin, V. P. Recent advances with liposomes as pharmaceutical carriers. *Nat Rev Drug Discov* **4,** 145–160 (2005).
42. Lee, S. H., Choi, S. H., Kim, S. H. & Park, T. G. Thermally sensitive cationic polymer nanocapsules for specific cytosolic delivery and efficient gene silencing of siRNA: Swelling induced physical disruption of endosome by cold shock. *Journal of Controlled Release* **125,** 25–32 (2008).

43. Duracher, D., Sauzedde, F., Elaïssari, A., Pichot, C. & Nabzar, L. Cationic amino-containing N-isopropyl- acrylamide-styrene copolymer particles: 2-surface and colloidal characteristics. *Colloid and Polymer Science* **276,** 920–929 (1998).
44. Smith, M. H. & Lyon, L. A. Multifunctional Nanogels for siRNA Delivery. *Acc. Chem. Res.* **45,** 985–993 (2012).
45. Blackburn, W. H., Dickerson, E. B., Smith, M. H., McDonald, J. F. & Lyon, L. A. Peptide-functionalized nanogels for targeted siRNA delivery. *Bioconjug. Chem.* **20,** 960–968 (2009).
46. Karg, M. *et al.* Thermoresponsive core–shell microgels with silica nanoparticle cores: size, structure, and volume phase transition of the polymer shell. *Phys. Chem. Chem. Phys.* **10,** 6708 (2008).
47. Greenberg, S. A. The depolymerization of silica in sodium hydroxide solutions. *The Journal of Physical Chemistry* **61,** 960–965 (1957).
48. Richtering, W., Dubbert, J., Gelissen, A. P. H., Lindner, P. & Schmid, A. J. Structure determination of microcapsules with advanced temperature responsive behavior. *Institut Laue-Langevin (ILL)*, doi: 10.5291/ILL-DATA.9-11-1706 (2014).
49. Pedersen, J. S., Posselt, D. & Mortensen, K. Analytical treatment of the resolution function for small-angle scattering. *J Appl Crystallogr* **23,** 321–333 (1990).
50. Berndt, I., Pedersen, J. S. & Richtering, W. Structure of multiresponsive 'intelligent' core-shell microgels. *J. Am. Chem. Soc.* **127,** 9372–9373 (2005).
51. Berndt, I., Pedersen, J. S. & Richtering, W. Temperature-sensitive core-shell microgel particles with dense shell. *Angew. Chem. Int. Ed. Engl.* **45,** 1737–1741 (2006).
52. Plimpton, S. Fast parallel algorithms for short-range molecular dynamics, *J. Comp. Phys.* **117,** 1–19 (1995).
53. Kobayashi, H. & Winkler, R. G. Structure of microgels with Debye-Hückel interactions. *Polymers* **6,** 1602–1617 (2014).
54. Rumyantsev, A. M., Rudov, A. A. & Potemkin, I. I. Intraparticle segregation of structurally homogeneous polyelectrolyte microgels caused by long-range coulomb-repulsion. *J. Chem. Phys.* **142,** 171105 (2015).
55. Toxvaerd, S. & Dyre, J. C. Shifted forces in molecular dynamics. *J. Chem. Phys.* **134,** 081102 (2011).
56. Schroeder, R. *et al.* Electrostatic interactions and osmotic pressure of counterions control the pH-dependent swelling and collapse of polyampholyte microgels with random distribution of ionizable groups. *Macromolecules* **48,** 5914–5927 (2015).
57. Stieger, M., Richtering, W., Pedersen, J. S. & Lindner, P. Small-angle neutron scattering study of structural changes in temperature sensitive microgel colloids. *J. Chem. Phys.* **120,** 6197–6206 (2004).

Acknowledgements

We thank Katja Nothdurft for help with the synthesis. The authors thank the Deutsche Forschungsgemeinschaft (DFG) for funding within the SFB 985 "Functional Microgels and Microgel Systems". M.K. acknowledges funding through the Deutsche Forschungsgemeinschaft (DFG) within the SFB 840. A.A.R. and I.I.P. gratefully acknowledge financial support of the Russian Foundation for Basic Research within the projects 15-33-21151 and 16-03-00352. Simulations were performed on multi-petaflops "Lomonosov" supercomputer at Moscow State University.

Author Contributions

A.J.S. performed the SANS experiments, analyzed the scattering curves and wrote the manuscript. J.D. supervised the synthesis of the particles and performed the SANS measurements. A.R. performed the simulations, graphic design and wrote the manuscript. J.S.P. developed the fitting model and provided a fitting program. P.L. also contributed to the SANS measurements. M.K. synthesized the silica core and the core-shell particles. W.R. and I.P. conceived the concept, discussed the results and wrote the manuscript. All authors approved the final version of the manuscript.

Additional Information

Supplementary information accompanies this paper at http://www.nature.com/srep

Competing financial interests: The authors declare no competing financial interests.

How to cite this article: Schmid, A. J. *et al.* Multi-Shell Hollow Nanogels with Responsive Shell Permeability. *Sci. Rep.* **6**, 22736; doi: 10.1038/srep22736 (2016).